Available online at www.sciencedirect.com
SCIENCE DIRECT
ELSEVIER
polymer
Polymer 46 (2005) 6959–6967
www.elsevier.com/locate/polymer

Photosensitive polyimide/silica hybrid optical materials: Synthesis, properties, and patterning

Yu-Wen Wang[a], Cheng-Tyng Yen[b], Wen-Chang Chen[a,b,*]

[a]*Institute of Polymer Science and Engineering, National Taiwan University, Taipei 106, Taiwan, ROC*
[b]*Department of Chemical Engineering, National Taiwan University, Taipei 106, Taiwan, ROC*

Received 2 May 2005; received in revised form 9 June 2005; accepted 13 June 2005
Available online 12 July 2005

Abstract

In conventional ionic salt photosensitive polyimides, large volume shrinkage during imidization would be occurred due to eliminating pendant photosensitive moieties, such as 2-methyl acrylic acid 2-dimethylamino-ethyl ester (MDAE). In this study, the volume shrinkage of photosensitive poly(4,4′-(hexafluoroisopropylidenediphthalic anhydride)-*co*-oxydianiline) (6FDA-ODA)/MDAE was largely reduced by photocrosslinking MDAE with a coupling agent and the silica domain in the hybrid materials. The used coupling agents were 3-methacryloxypropyl trimethoxysilane (MPTMS) or (4-vinylphenethyl)trimethoxysilane (VPTMS). The coupling agent and the silica domain are designed primarily for reducing the volume shrinkage and enhancing the thermal properties, respectively. The retention of MDAE in the prepared hybrid films is supported by X-ray photoelectron spectroscopy (XPS) and thickness variation during curing process. The silica domain in the hybrid materials from TEM analysis was in the range of 10–50 nm, which was formed by the coupling agent and tetramethoxysilane. The silica domain significantly enhanced the thermal properties of the prepared hybrid films in comparison with parent fluorinated polyimide, including the glass transition temperature and coefficient of thermal expansion. The prepared hybrid materials also exhibited reduced refractive index and optical loss by increasing the silica. The SEM diagram suggested the prepared photosensitive hybrid materials could obtain lithographical patterns with a good resolution. These results indicate that the newly prepared photosensitive polyimide/silica hybrid materials may have potential applications for optical devices.
© 2005 Elsevier Ltd. All rights reserved.

Keywords: Photosensitive; Hybrid materials; Optical properties

1. Introduction

Organic–inorganic hybrid materials have been recognized as a new class of advanced materials because they can produce superior properties over the parent organic or inorganic materials [1–7]. Polyimide-silica hybrid materials have been widely studied recently due to their excellent thermal, mechanical, and electronic properties [8–23]. In these reports, the control of polyimide and silica domain size have been addressed by the approach of enhancing coupling density by short chain polyimide segment, coupling agents, or interchain coupling. Besides the enhanced thermal/mechanical properties, the optical properties of polyimides could be tuned through the silica moiety, including refractive index, extinction coefficient, optical birefringence, and optical loss [20–22].

Incorporation of photosensitive functionality into hybrid materials is essential for patterned optoelectronic devices since it can save the extra step of adding photoresists. However, only limited polyimide/oxide hybrid materials have been demonstrated to be photopatternable. For example, Zhu et al. prepared the polyimide/silica hybrid materials based on intrinsic photosensitive dianhydride moiety of 3,3′,4,4′-benzophenonetetracarboxylic dianhydride (BTDA) [24]. Later, they extended a similar approach to prepare photosensitive polyimide/titania materials [25,26]. Although these are among the first few reports on photosensitive polyimide/inorganic hybrid materials, the patterned resolution (10 μm) and relatively large inorganic particle size (300 nm–2 μm) could be further explored. Ionic salt or ether type photosensitive

* Corresponding author. Address: Department of Chemical Engineering, National Taiwan University, Taipei 106, Taiwan, ROC. Tel.: +886 2 23628398; fax: +886 2 23623040.
E-mail address: chenwc@ntu.edu.tw (W.-C. Chen).

0032-3861/$ - see front matter © 2005 Elsevier Ltd. All rights reserved.
doi:10.1016/j.polymer.2005.06.026

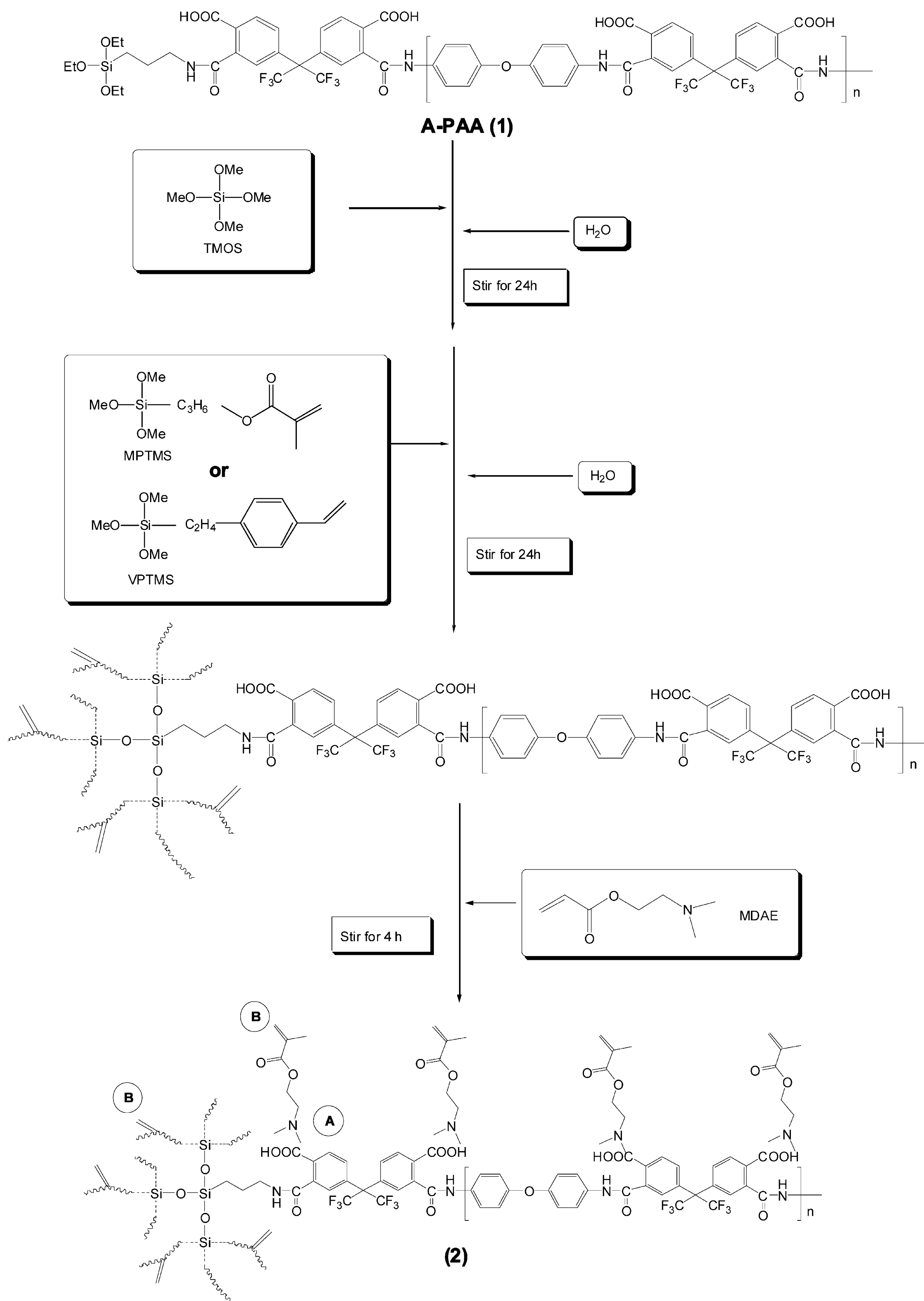

Scheme 1.

polyimides (PSPI) are widely used in microelectronic industries, including printed circuit boards (PCB) and electronic packing. However, their applications on opto-electronic devices (e.g. optical waveguides) are significantly limited because a large volume shrinkage after curing (often up to 20–50%) is occurred from eliminating pendant photosensitive moieties. Such large volume shrinkage would cause a significant distortion on the patterned feature (usually rounded edge) [27], reduced critical resolution and induced large thermal stress after heat treatments. Hence, the reduction of volume shrinkage has become one of the major issues for photosensitive polyimides. Besides, thermal and mechanical properties of organic polyimides need to be enhanced for optoelectronic applications. The approach of preparing photosensitive polyimide/silica hybrid materials could resolve the above problems of ionic salt photosensitive polyimide materials for optoelectronic devices.

In this study, novel ionic-salt type photopatternable fluorinated polyimide/silica hybrid materials were developed to reduce the volume shrinkage and enhance physical properties over conventional photosensitive polyimides, as illustrated in Scheme 1. APrTEOS-Capped poly(amide acid)–silica precursor (**A-PAA**, **1**) was synthesized by 4,4′-hexafluoroisopropylidenediphthalic anhydride (6FDA) and oxydianiline (ODA), followed by reacting with aminopropyltriethoxysilane (APrTEOS). Then, the **A-PAA** was reacted with tetramethoxysilane (TMOS) and then de-ionized water was added. After that, 3-methacryloxypropyl trimethoxysilane (MPTMS) or (4-vinylphenethyl)trimethoxysilane (VPTMS) was reacted to the TMOS-developed silica clusters in the solution. Then, the 2-methyl acrylic acid 2-dimethylamino-ethyl ester (MDAE) and photo-initiator, Irgacure-819 were added to form the precursor (**2**) of the photosensitive polyimide/silica hybrid **P1**∼**P3c** films. The MDAE was protonated as an acid/base ionic pair on the PAA moiety, as shown in **A** of the precursor (**2**) of Scheme 1. The precursors (**2**) were then used for lithographic patterning process to develop the target pattern, followed by curing for the imidization of the amic acid moiety. The role of MPTMS or VPTMS is to enhance dimension stability by photocrosslinking with MDAE and simultaneously incorporated with the silica domains developed by TMOS, as shown in **B** of (**2**) of Scheme 1. The silica domain may contribute to prevent the evaporation of MDAE as well as enhance the thermal properties. The effects of coupling agent and the silica content on the morphologies and physical properties of the obtained hybrid materials were discussed. The lithographic patterns of the prepared hybrid materials were characterized by SEM.

2. Experimental

2.1. Materials

4,4′-Hexafluoroisopropylidenediphthalic anhydride (6FDA, Lancaster, 99%) was purchased and dehydrated at 120 °C under reduced pressure. Oxydianiline (ODA, Acros, 99%) was purchased and purified by sublimation. 3-Aminopropyl triethoxysilane (APrTEOS, Aldrich, 97%), 2-methyl acrylic acid 2-dimethylamino-ethyl ester (MDAE, Aldrich, 98%), tetramethyl orthosilicate (TMOS, Aldrich, 99%), 3-methacryloxypropyl trimethoxysilane (MPTMS, Aldrich, 98%), 4-vinylphenethyltrimethoxysilane (VPTMS, Gelest, 99%), and *N*,*N*-dimethyl acetamide (DMAc, Tedia, 99%) were purchased and used without purification. The photo-initiator, bis(2,4,6-trimethylbenzoyl) phenyl phosphine oxide (Irgacure-819) was grateful provided by CIBA Geigy of Taiwan.

*2.2. Preparation of the photosensitive APrTEOS-capped poly(amide acid)–silica precursor(**A-PAA**)*

Briefly, APrTEOS-capped poly(amide acid)–silica precursor (**A-PAA**) was synthesized by the 4,4′-hexafluoro-isopropylidenediphthalic anhydride (6FDA) with oxydianiline (ODA) and then coupled with 3-aminopropyl triethoxysilane (APrTEOS) at the mole ratio of 5:4:2, respectively. The synthetic procedures were reported previously by our laboratories [20–22].

Table 1
The molar ratios of compositions on the reaction mixtures and their resulted film compositions

	Molar ratio of the composition[a,b]							Film composition (%)	
	6FDA	ODA	APrTEOS	TMOS	MTPMS	VPTMS	MDAE	Polyimide	Silica
P1	5	4	2	0	0	0	10	97.5	2.5
P2a	5	4	2	0	5	0	10	92.7	7.3
P2b	5	4	2	3	5	0	10	90.0	10.0
P2c	5	4	2	5	5	0	10	88.3	11.7
P3a	5	4	2	0	0	5	10	92.8	7.2
P3b	5	4	2	3	0	5	10	91.2	9.8
P3c	5	4	2	5	0	5	10	88.5	11.5

[a] PAA 15% in NMP.
[b] The amount of added water was equal to the total moles of the Si–OR groups from APrTEOS, TMOS, and MPTMS (or VPTMS).

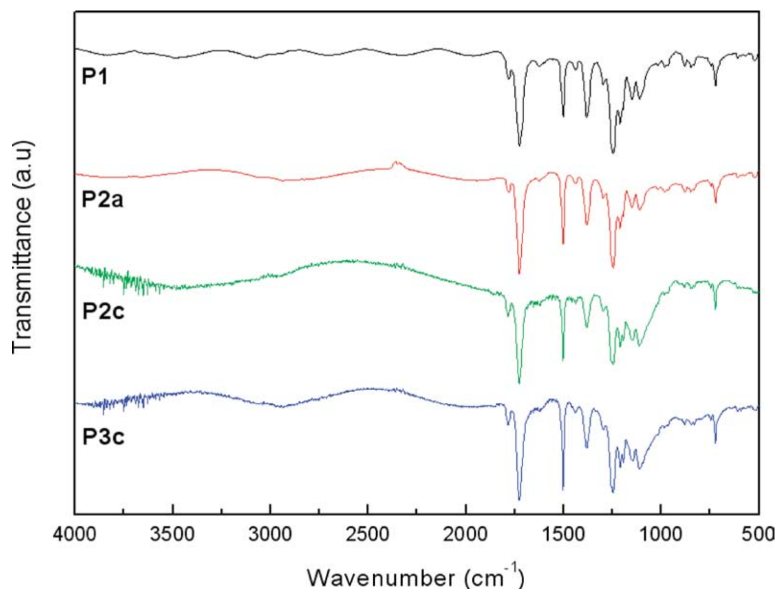

Fig. 1. FTIR spectra of prepared thin films, **P1a**, **P2a**, **P2c**, and **P3c** on silicon wafer.

*2.3. Preparation of the precursor solutions (**2**, in Scheme 1) of the hybrid films, **P1∼P3c***

The compositions for preparing photosensitive PI-silica films, **P1∼P3c**, are listed in Table 1. By using **P2c** as an example, 912 mg of the TMOS (6 mmol) was added to the **A-PAA** solution, and stirred for 15 min as shown in Scheme 1. Then de-ionized water was added and allowed to react at room temperature for another 24 h. The amount of added water was equal to the total moles of the Si–OR groups for APrTEOS, TMOS, and MPTMS. After that, 1394 mg (6 mmol) of the MPTMS was added and allowed to react at room temperature for 4 h. In the following, 3144 mg (20 mmol) of the MDAE and 136 mg of Irgacure-819 was added and stirred for 2 h to form the precursor of the **P2c**.

2.4. Lithographic patterning

The prepared precursors of the **P1∼P3c** were spin-coated onto a 4 in silicon wafer at 1500 rpm for 20 s. The thin film was then soft-baked at 90 °C for 4 min to evaporate partial solvents, then exposed to the UV light of 365 nm (I-line) through a transparent mask (for FTIR, prism coupler, XPS, and TEM measurement) or a pre-defined Cr mask with the dose of 1800 mJ/cm^2. The films were post-exposure-baked (PEB) at 90 °C for 2 min, and then developed by the mixture of γ-butyrolactone/DMSO/H_2O in the weight ratio of 42/50/8. Finally, the developed pattern was cured by the multi-step heating process of 150, 200, 250, and 300 °C for 30 min each on a hot plate.

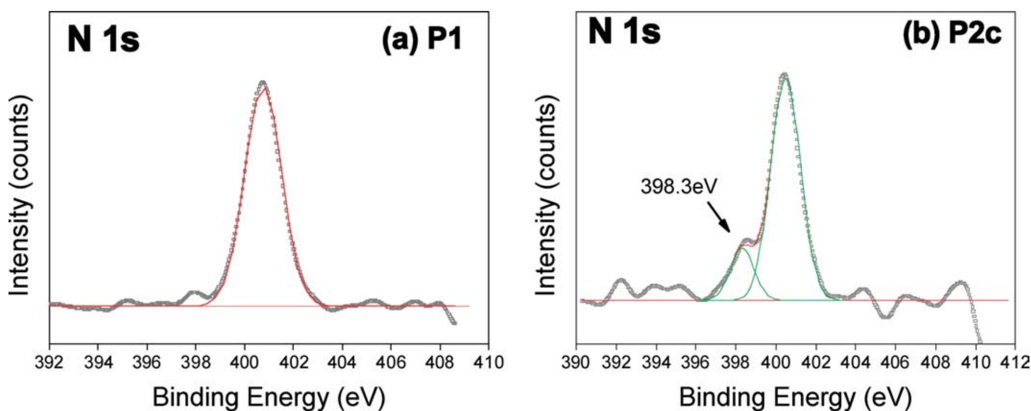

Fig. 2. XPS N1s core-level spectra of the prepared films, (a) **P1** (b) **P2c**.

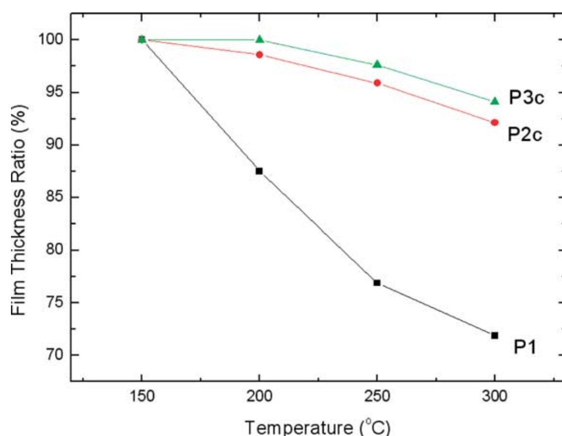

Fig. 3. Thickness variation of the **P1**, **P2c**, and **P3c** in the curing process.

2.5. Characterization

The FTIR and near-infrared (NIR) absorption spectra of the prepared films were recorded by a DIGILAB FTS-3500GX spectrophotometer. The preparation of the hybrid films for the NIR absorption measurement was described as below. The precursor solution was poured into a Teflon tray, baked at 150 °C for 30 min, expose to UV light (Hg lamp) for another 30 min, and then cured at 200/250/300 °C for 30 min each to produce free-standing dry film (∼300–400 μm), for the characterization of near-infrared (NIR) absorption and thermal properties. Photoelectron (XPS) spectrum was obtained using a VG Microscan MT-500 ESCA system with the primary excitation source of non-monochromatic Mg Kα (300 W, 1253.6 eV). The window and number of sweeps used for N1s were 390–410 eV and 20 sweeps. The constant pass energy and step size were 20 and 0.05 eV, respectively. The SEM pictures of lithographic patterns were obtained by a JEOL JSM-5310 microscope. The TEM diagram was obtained from the JEOL (model number: 2002-EX).

The thermal decomposition temperatures (T_d) and glass transition temperature (T_g) of the prepared materials were obtained by a TA Instrument TGA 951 thermogravimetric analyzer (TGA) and a DSC 910S differential scanning calorimeter (DSC) at a heating rate of 10 and 20 °C/min under nitrogen atmosphere, respectively. T_d (e.g. T_{d1}, T_{d2} in Fig. 4) determined by the intersection of the tangent lines of transition steps in the TGA curve. A TA2940 thermomechanical analyzer (TMA) was used to characterize coefficient of thermal expansion (CTE) from 40 to 200 °C at a heating rate of 10 °C/min. A Metricon Model 2100 prism coupler was used to measure the thickness (T) and refractive indices of the prepared thin films at the wavelength of 1319 nm. A NanoScope III atomic force microscope (AFM) was used to measure the average roughness (R_a) and root mean square roughness (R_q) of the thin films on silicon wafer. The propagation losses of the prepared waveguides at the wavelength of 1310 and 1550 nm were measured using the silicon oxide as the cladding layer by a cut-back method according to our previous reports [20–22].

3. Results and discussion

Fig. 1 shows the FTIR spectra of the prepared films, **P1**, **P2a**, **P2c**, and **P3c**, after curing. The C–NH (1660 cm^{-1}) and Si–OH (around 3500 cm^{-1}) characteristic absorption band are completely disappeared in all spectra, which indicate the fully imidization of PAA and condensation of silica domain, respectively. The imide characteristic absorption bands of the prepared materials are further evidenced by the following absorption bands: 1778 cm^{-1} (C=O sym. str.); 1726 cm^{-1} (C=O asym. str.); and 1380 cm^{-1} (C–N str.) The stronger Si–O–Si stretching band around 1100 cm^{-1} of **P2c** or **P3c** than that of **P1** or **P2a** suggests the higher silica content in the former consistent with that shown in Table 1.

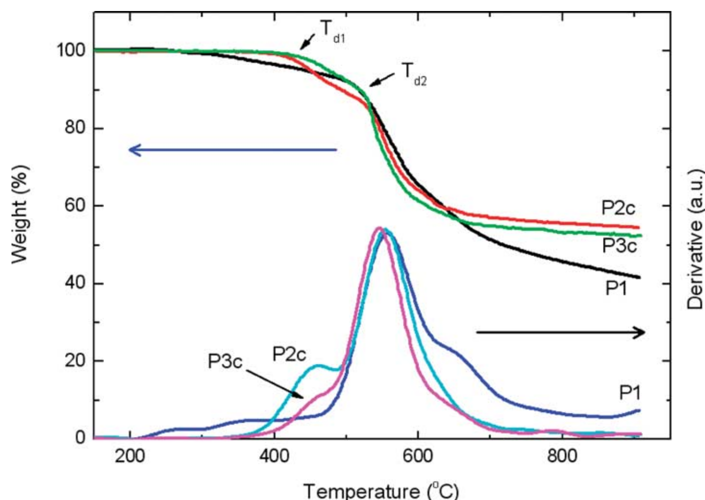

Fig. 4. TGA curves of the **P1**, **P2c**, and **P3c** at the heating rate of 10 °C/min under nitrogen atmosphere.

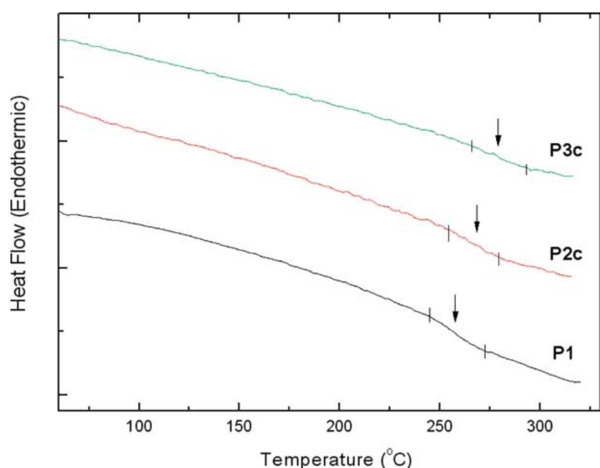

Fig. 5. DSC curves of the **P1**, **P2c**, and **P3c** at a heating rate of 20 °C/min under nitrogen atmosphere.

The retention of MDAE by the coupling agent, MPTMS or VPTMS, is important for reducing the volume shrinkage. Fig. 2(a) and (b) shows the N1s core-level of the **P1** and **P2c**, respectively. Both figures show the same peak at the binding energy of 400.5 eV, which is assigned to the characteristic peak of nitrogen on polyimide backbone [28]. However, there is a new peak at the binding energy 398.3 eV appeared in Fig. 2(b) but absent in Fig. 2(a), which is assigned to nitrogen of tertiary amine of MDAE [29]. It suggests that the retention of the MDAE in the hybrid film by photocrosslinking with MPTMS in **P2c**. However, the observance of no or insignificant residue MDAE in the **P1** film from Fig. 2(a) is as expected since there is no coupling agent in the composition.

The retention of MDAE in the studied films could be further studied by the variation of film thickness during imidization. Fig. 3 shows the thickness variation of **P1**, **P2c**, and **P3c** at various curing temperatures. The film thickness ratio was defined as the film thickness after each baking step over the initial thickness (T_0). The T_0 is defined as the film thickness after the first baking step (150 °C for 30 min) and used as the reference for eliminating the effect of residue solvents (NMP) in film. The volume shrinkage of the prepared hybrid films, **P1 ~ P3c**, is resulted from eliminating the photoactive group or water during imidization in the temperature of 150–300 °C. Note that the imidization is generally occurred in the above temperature range. As shown in the figure, the film thickness ratio is only 71.9% in the case of **P1** but 92.1 and 94.1% are obtained for the **P2c** and **P3c** after curing at 300 °C, respectively. The large volume shrinkage of 28.1% on **P1** is probably resulted from the elimination of MDAE since the MDAE can only kept in film as the acid/base ionic pair with carboxylic acid of amic acid moiety. However, the volume shrinkages of **P2c** and **P3c** were significantly reduced by the covalent bonding of MDAE with MPTMS and VPTMS through UV irradiation, respectively. The film thickness ratios after curing at 300 °C are 85.5, 90, 91.3, and 91.5% for **P2a**, **P2b**, **P3a**, and **P3b**, respectively. It suggests that the silica content or the type of coupling agent could prevent on elimination of MDAE or reduce the volume shrinkage of the film by enhancing thermal/mechanical properties.

Figs. 4 and 5 show the TGA and DSC curves of the hybrid materials, **P1**, **P2c** and **P3c** after curing, respectively. The physical properties of the studied hybrid materials are listed in Table 2. The TGA curves show two decomposition transitions (T_{d1}, T_{d2}) in the **P2c** and **P3c**, but just one in the **P1**. The differential thermogravimetric (DTG) curves in Fig. 4 also show the same characteristic as the TGA curves. Such kind of two degradation temperatures was found in all of the hybrid materials of **P2a ~ P3c**. The lower T_{d1} is probably resulted from the decomposition of the photocrosslinking moiety of MDAE with MSMA or SETMOS while the higher T_{d2} is suggested to be the decomposition of the polyimide backbone. As shown in Table 2, the higher decomposition temperatures of **P2a ~ P3c** are in the range of 517–528 °C, which is higher than the parent **P1** due to the incorporation of the silica moiety. The T_{d2} of the **P3a ~ P3c** are higher than those of the corresponding **P2a ~ P2c**. It suggests that the coupling agent of VPTMS with the aromatic ring structure could result in a higher thermal stability than the MPTMS for the hybrid materials. The DSC curve of the **P1** shows a T_g at 258 °C but that of the **P3c** shows a broad and featureless T_g at 282 °C. It suggests that the incorporating silica content could limit the segmental motion and thus enhance the thermal stability, which are similar to that reported on other hybrid materials [30]. Fig. 6 shows the TMA curves of the studied materials, **P1**, **P2a**, **P2c**, and **P3c**. The significantly lower coefficient of thermal expansion (CTE) of the **P2c** (23.7 ppm/°C) and **P3c**

Table 2
The physical properties of of the prepared films, **P1 ~ P3c**

	Thermal properties					Roughness		Optical properties			
	$T_{d,1}$ (°C)	$T_{d,2}$ (°C)	T_g (°C)	CTE (ppm/°C)	T (nm)	R_a (nm)	R_q (nm)	n_{TE}^{1319}	n_{TM}^{1319}	Δn	α^{1319} (dB/cm)
P1	–	515	258	45.0	2874	1.185	1.573	1.558	1.545	0.013	1.04
P2a	390	520	220	107.0	2446	0.847	1.074	1.545	1.539	0.006	0.86
P2b	405	524	237	40.8	2102	0.550	0.754	1.538	1.535	0.003	0.83
P2c	415	528	264	23.7	1950	0.491	0.619	1.538	1.534	0.004	0.80
P3a	410	517	235	33.0	1746	0.506	0.619	1.560	1.553	0.007	0.93
P3b	425	525	248	30.9	3507	0.453	0.567	1.550	1.545	0.005	0.86
P3c	430	527	282	21.8	3215	0.416	0.510	1.548	1.543	0.005	0.82

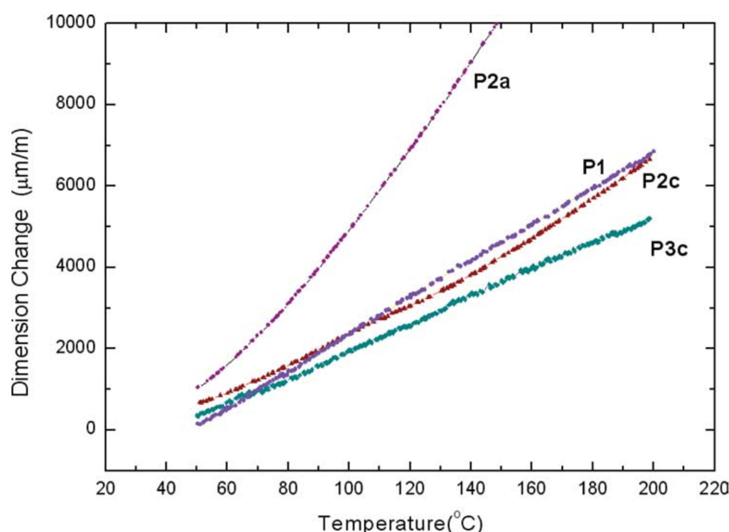

Fig. 6. TMA curves of the **P1**, **P2a**, **P2c**, and **P3c** at a heating rate of 10 °C/min under nitrogen atmosphere.

(21.8 ppm/°C) than that of **P1** (45.0 ppm/°C) are shown in the figure and Table 2. However, the CTE of the **P2a** are much higher than that of **P1** due to the long alkyl moiety from MPTMS and MDAE remained in the materials. The T_g of the hybrid materials could be lower than the parent polyimide for the case of low silica fractions in the **P2a**, **P2b**, **P3a**, and **P3b**. It suggests that the silica content plays a very important role for enhancing the thermal/mechanical properties of the parent polyimides. The higher T_g or lower CTE of the hybrid materials with the VPTMS than that with MPTMS again suggests the significance of the chemical structure of the coupling agent on the thermal stability. Hence, selection of proper coupling agent and optimum silica content should be considered for design hybrid materials.

The thickness (T), average roughness (R_a) and root mean square roughness (R_q) of the prepared films are shown in Table 2. The average roughness (R_a) and root mean square roughness (R_q) of the prepared films are mostly less than 1 nm for **P2a** ~ **P3c**. It suggests that the prepared films have an excellent surface planarity in comparison of their film thickness of 1746–3507 nm. The smaller R_a and R_q of **P2c** and **P3c** than that of **P1** (>1 nm) is probably because the large silica content in the former improves the adhesion between the prepared materials and the silicon substrate. TEM picture of **P2c** shown in Fig. 7 reveals that the average particles size of silica is in the range of 10–50 nm with the average of 34 nm. The silica domain size of the **P3c** is also in the similar range as that of the **P2c**. The Raleigh scattering loss induced such silica domain is suggested to be insignificant in the near-infrared wavelength regions [31]. The excellent planarity and small silica size of the prepared films suggests the potential optical applications.

The optical properties of the prepared films are summarized in Table 2. The refractive indices of the

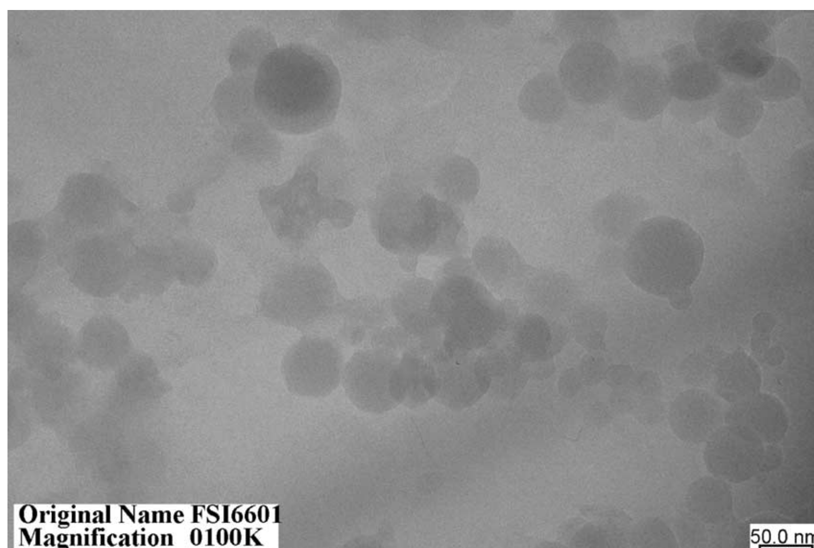

Fig. 7. The TEM diagram of the **P2c** film.

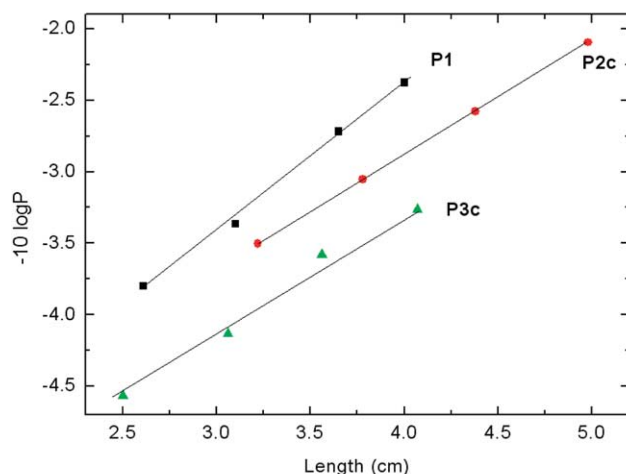

Fig. 8. Variation of the transmitted optical power ($-10\log P$) with the lengths of the **P1**, **P2c**, and **P3c** films on silicon wafer.

transverse electric refractive indices (n^{TE}) and transverse magnetic refractive indices (n^{TM}) at 1319 nm are generally less than 1.560 with the decreasing trend of increasing silica content. The lower refractive index of the silica than that of the polyimide moiety results in such trend. The birefringences (n^{TE}–n^{TM}) of the prepared films are also reduced with increasing the silica. It indicates that the silica could inhibit the orientation of polyimide backbone along the substrate surface and thus explains the above trend on birefringence. Hence, the incorporation of the silica moiety into polyimides could not only reduce the refractive index but also the birefringence.

Fig. 8 shows the variation of transmitted optical power ($-10\log P$) with the length of the prepared films. The propagation optical losses (α^{1319}) of the prepared films at 1319 nm determined by the cut-back method of Fig. 8 are listed in Table 2. The optical loss of the **P1**, **P2a ~ P2c**, and **P3a ~ P3c** are 1.04, 0.86–0.80, 0.93–0.82 dB/cm, respectively. It suggests the incorporation of silica to the polyimide reduces the optical loss by decreasing the C–H number density. Note that the NIR absorption spectrum shows three absorption peaks around 1660 ($2\nu_{C-H}$), 1410($2\nu_{C-H}+\delta_{C-H}$), and 1130 ($3\nu_{C-H}$) nm [32]. It also indicates that the silica domain would not result in a significant scattering loss.

Fig. 9 shows the SEM diagrams of the developed pattern of **P2c** and **P3c**. Both **P2c** and **P3c** show a clear edge on the diagrams, which suggest both **P2c** and **P3c** with good dimensional stability. Based on the optical properties and patterning resolution, the prepared hybrid materials of **P2c** and **P3c** could have potential applications for channel optical waveguides. It also indicates that the approach of crosslinking MDAE with coupling agent (MSMA or SETMOS) and incorporating silica moiety could significantly reduce the volume shrinkage and thus a good patterning resolution is obtained. The present approach of reducing the volume shrinkage as well as enhancing thermal/mechanical properties could be easily applied to other hybrid materials for device applications [33]. It also stands for the potential of applying to those active polyimide/ceramic hybrid materials, such as non-linear optical [34] and luminescent materials [35], to develop novel multifunctional high performance materials.

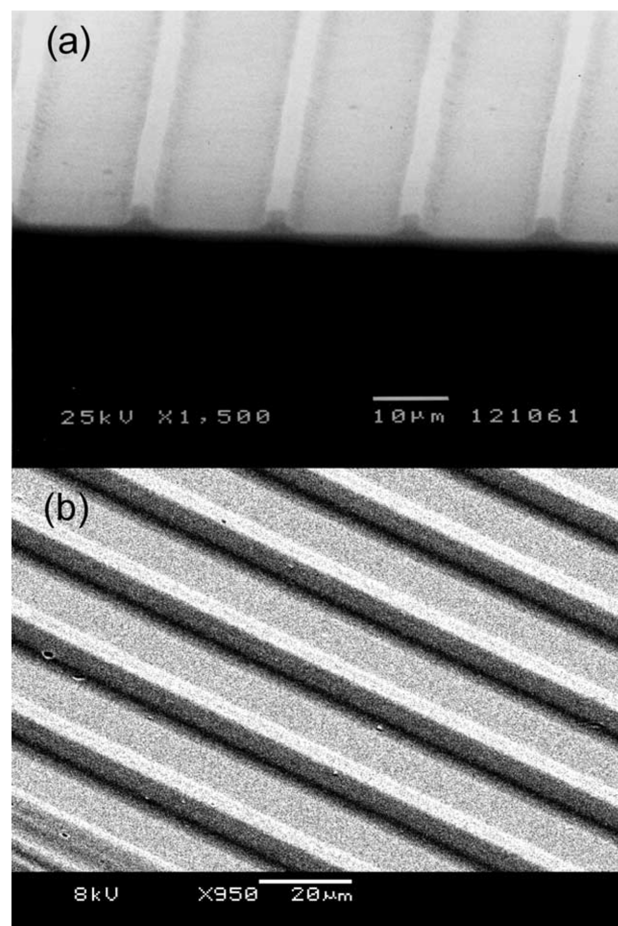

Fig. 9. SEM diagrams on the developed patterns of (a) **P2c** (3×3 μm^2) and (b) **P3c** (5×3 μm^2).

4. Conclusions

In summary, we have successfully prepared new photosensitive fluorinated polyimide/silica hybrid materials. The novel photosensitive polyimide/silica hybrid materials could largely eliminate the evaporation of MDAE during curing using coupling agent and silica. Thus, large volume shrinkage exhibited in conventional ionic type photosensitive polyimide could be resolved by the present approach. The silica domain in the hybrid materials also significantly enhanced the thermal properties. It also exhibits good lithographic resolution, dimensional stability, and low optical loss in the NIR region. The newly prepared photosensitive materials could have potential applications for patterned electronic and optoelectronic devices.

Acknowledgements

We thank the financial support of National Science Council, and the Ministry of Economic Affairs of Taiwan for this work.

References

[1] Tamaki R, Tanaka Y, Asuncion MZ, Choi J, Laine RM. J Am Chem Soc 2001;123:12416.
[2] Sanchez C, Lebeau B. MRS Bull 2001;26:377.
[3] Kagan CR, Mitzi DB. Science 1999;286:945.
[4] Huynh WU, Dittmer JJ, Alivisatos AP. Science 2002;295:2425.
[5] Tessler N, Medveder V, Kazes M, Kan S, Banin U. Science 2002;295:1506.
[6] Lee LH, Chen WC. Chem Mater 2001;11:1137.
[7] Lin WJ, Chen WC, Wu WC, Niu YH, Jen AKY. Macromolecules 2004;37:2335.
[8] Nandi M, Conklin JA, Salvati L, Sen A. Chem Mater 1991;3:201.
[9] Morikawa A, Yamaguchi H, Kakimoto M, Imai Y. Chem Mater 1994;6:913.
[10] Wang S, Ahmad Z, Mark JE. Chem Mater 1994;6:943.
[11] Schrotter JC, Smaihi M, Guizard C. J Appl Polym Sci 1996;61:2137.
[12] Srinivasan SA, Hedrick JL, Miller RD, DiPietro R. Polymer 1997;38:3129.
[13] Sysel P, Pulec R, Maryska M. Polym J 1997;29:607.
[14] Chen Y, Iroh JO. Chem Mater 1999;11:1218.
[15] Mascia L, Kioul A. Polymer 1995;36:3649.
[16] Ahmad Z, Mark JE. Chem Mater 2001;13:3320.
[17] Tsai MH, Whang WT. Polymer 2001;42:4197.
[18] Cornelius CJ, Marand E. Polymer 2002;43:2385.
[19] Shang XY, Zhu ZK, Yin J, Ma XD. Chem Mater 2002;14:71.
[20] Chang CC, Chen WC. Chem Mater 2002;14:4242.
[21] Chang CC, Wei KH, Chang YL, Chen WC. J Polym Res 2003;10:1.
[22] Yen CT, Chen WC, Liaw DJ, Lu HY. Polymer 2003;44:7097.
[23] Chang CC, Wei KH, Chen WC. J Electrochem Soc 2003;150:F147.
[24] Zhu ZK, Yin J, Cao F, Shang XY, Lu QH. Adv Mater 2000;12:1055.
[25] Liu L, Lu Q, Yin J, Zhu Z, Pan D, Wang Z. Mater Sci Eng C 2002;22:61.
[26] Liu L, Lu Q, Yin J, Qian X, Wang W, Zhu Z, et al. Mater Chem Phys 2002;74:210.
[27] Kataoka F, Suzuki H. In: Horie K, Yamashita T, editors. Photosensitive polyimides. Lancaster: Technomic; 1995.
[28] Fu GD, Wang WC, Li S, Kang ET, Neoh KG, Tseng WT, et al. J Mater Chem 2003;13:2150.
[29] Jansen RJJ, van Bekkum H. Carbon 1995;33:1021.
[30] Lee SJ, Chen WC. Polym J 2000;32:67.
[31] Hunsperger RG. Integrated optics, theory and technology. Berlin: Springer; 1991.
[32] Yen CT, Chen WC. Macromolecules 2003;36:3315.
[33] Sanchez C, Lebeau B, Chaput F, Boilot JP. Adv Mater 2003;15:1969.
[34] Marturunkakul S, Chen JI, Jeng RJ, Sengupta S, Kumar J, Tripathy SK. Chem Mater 1993;5:743.
[35] Kuriki K, Koike Y, Okamoto Y. Chem Rev 2002;102:2347.